

Error correlations in photonic qudit-mediated entanglement generation

Liu, Xiaoyu; Bharos, Niv; Markovich, Liubov; Borregaard, Johannes

DOI

[10.1103/PhysRevResearch.6.023075](https://doi.org/10.1103/PhysRevResearch.6.023075)

Publication date

2024

Document Version

Final published version

Published in

Physical Review Research

Citation (APA)

Liu, X., Bharos, N., Markovich, L., & Borregaard, J. (2024). Error correlations in photonic qudit-mediated entanglement generation. *Physical Review Research*, *6*(2), Article 023075. <https://doi.org/10.1103/PhysRevResearch.6.023075>

Important note

To cite this publication, please use the final published version (if applicable). Please check the document version above.

Copyright

Other than for strictly personal use, it is not permitted to download, forward or distribute the text or part of it, without the consent of the author(s) and/or copyright holder(s), unless the work is under an open content license such as Creative Commons.

Takedown policy

Please contact us and provide details if you believe this document breaches copyrights. We will remove access to the work immediately and investigate your claim.

Error correlations in photonic qudit-mediated entanglement generation

Xiaoyu Liu^{1,2,*}, Niv Bharos^{2,3,†}, Liubov Markovich^{1,2,4,5,‡} and Johannes Borregaard^{2,6,§}

¹*Instituut-Lorentz, Universiteit Leiden, P.O. Box 9506, 2300 RA Leiden, The Netherlands*

²*QuTech and Kavli Institute of Nanoscience, Technische Universiteit Delft, Lorentzweg 1, 2628CJ Delft, Netherlands*

³*Research Laboratory of Electronics, Massachusetts Institute of Technology, Cambridge, Massachusetts 02139, USA*

⁴*Institute for Information Transmission Problems, Bolshoi Karetny pereulok 19, Moscow 127051, Russia*

⁵*Russian Quantum Center, Skolkovo, Moscow 121205, Russia*

⁶*Department of Physics, Harvard University, 17 Oxford Street, Cambridge, Massachusetts 021388, USA*



(Received 3 December 2023; accepted 1 March 2024; published 22 April 2024)

Generating entanglement between distributed network nodes is a prerequisite for the quantum internet. Entanglement distribution protocols based on high-dimensional photonic qudits enable the simultaneous generation of multiple entangled pairs, which can significantly reduce the required coherence time of the qubit registers. However, current schemes require fast optical switching, which is experimentally challenging. In addition, the higher degree of error correlation between the generated entangled pairs in qudit protocols compared to qubit protocols has not been widely studied in detail. We propose a qudit-mediated entangling protocol that completely circumvents the need for optical switches at the expense of a lower success probability of the scheme. Furthermore, we quantify the amount of error correlation between the simultaneously generated entangled pairs and analyze the effect on entanglement purification algorithms and teleportation-based quantum error correction. We find that optimized purification schemes can efficiently correct the correlated errors, while the quantum error correction codes studied here perform worse than for uncorrelated error models.

DOI: [10.1103/PhysRevResearch.6.023075](https://doi.org/10.1103/PhysRevResearch.6.023075)

I. INTRODUCTION

Quantum networking enables new primitives such as information-theoretically secure communication [1], quantum sensing networks [2–4], and distributed quantum computation [5–7]. Furthermore, it provides a promising route towards scalable quantum computers via modular designs [8]. A prerequisite for these applications is the distribution of high-fidelity entanglement between the network nodes to enable the reliable transfer of quantum information by quantum teleportation.

Entanglement purification [9,10] and quantum error correction [11,12] are promising means to suppress the effect of noise in the generation of entanglement. Both methods require the generation of many entangled pairs between the nodes, which are combined to enable high-fidelity transfer of quantum information.

Recently, several entanglement distribution protocols based on time-bin photonic qudit encoding were proposed

for the simultaneous generation of multiple entangled pairs between network nodes [13–16]. In general, they follow the setup outlined in Fig. 1. First, a single-photon qudit encoded in time bins is entangled with Alice’s qubit registers. The photon is transmitted to Bob, where the same entangling operation is performed. A successful run of the protocol is heralded by the detection of the photon via a high-dimensional X -basis measurement. If a photon is detected, all qubits in the registers of Alice and Bob are entangled. This contrasts with conventional schemes based on photonic qubits, where entangled pairs are generated independently of each other. This leads to conventional schemes having much more demanding requirements on the coherence times of the qubits for the generation of multiple entangled pairs, as discussed in Ref. [13].

A significant experimental challenge of the schemes in Refs. [13–16] is the requirement of fast optical switches for routing of the photon to ensure the correct interaction with the qubits and to interfere the time bins in the final heralding measurement of the photon. The schemes also require a single photon to interact with all qubits, which can cause correlated errors between the entangled pairs. The extent of correlated errors and their effects on key applications such as entanglement purification and teleportation-based error correction have not been widely studied in detail.

In this paper, we propose a photonic qudit-mediated entanglement protocol that circumvents the use of optical switches, making it more accessible to the near-term hardware. This is obtained at the expense of the final X measurement being inherently probabilistic. However, we show how the success

*xiaoyu@lorentz.leidenuniv.nl

†niv@mit.edu

‡markovich@lorentz.leidenuniv.nl

§Corresponding author: borregaard@fas.harvard.edu

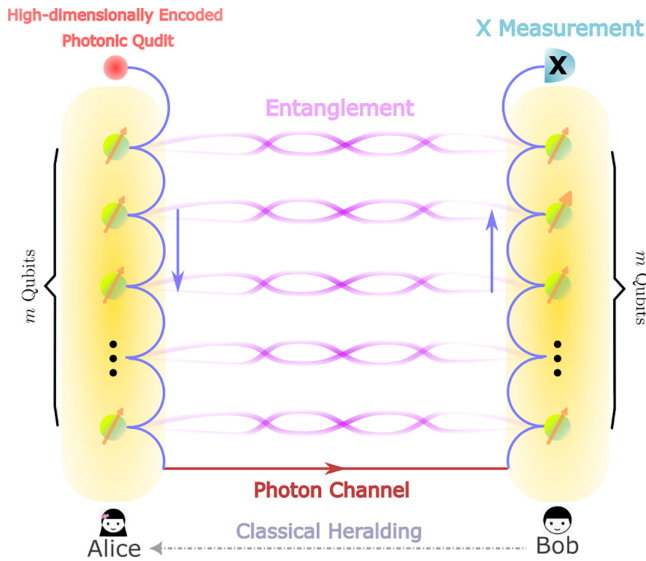


FIG. 1. General schematic of previous photonic qudit-mediated entanglement generation protocols [13–16]. Alice and Bob have registers with m qubits. A photonic qudit interacts first with Alice's and then with Bob's qubit registers. Bob performs a high-dimensional X -basis measurement of the photonic qudit. Heralded on the detection of a photon, m Bell pairs are generated simultaneously. Finally, Bob classically communicates to Alice whether or not the protocol succeeded.

probability can be boosted through a concatenated setup. We model and characterize the effect of correlated errors on the quality of the generated Bell pairs and apply optimized entanglement purification protocols [17] to distill high-fidelity entanglement. We also study the performance of teleportation-based quantum error correction, focusing on the $[[5,1,3]]$ and $[[4,2,2]]$ code [18–21]. We show that the optimized purification protocols can remove the correlated errors efficiently, while they have a more negative impact on the error correction codes.

II. SWITCH-FREE PROTOCOL

The goal of the qudit-mediated entanglement distribution protocol is to simultaneously generate m Bell pairs between Alice and Bob of the form

$$|\Phi^+\rangle^{\otimes m} = \frac{1}{2^{m/2}} (|0_A 0_B\rangle + |1_A 1_B\rangle)^{\otimes m}. \quad (1)$$

We show an overview of the proposed switch-free implementation in Fig. 2. The need for optical switches is circumvented in two parts of the protocol. First, previous protocols required optical switches to ensure the correct entangling procedure between the photonic time-bin qudit and the spins. This can, however, be circumvented by replacing the switches with local qubit rotations of the spins. Different from previous schemes, we let each time-bin pulse generated by Alice interact with all register qubits of both Alice and Bob through a single-sided cavity-mediated CZ gate between the photon (logical states $|0\rangle/|1\rangle$ corresponding to the absence/presence of the photon) and the qubits (logical states $|0\rangle/|1\rangle$ corresponding to a cavity noncoupled/coupled

spin state). We further discuss the physics of the CZ gate below.

Through single-qubit HADAMARD gates, we can control whether or not the presence of the photon in a time-bin pulse will flip the state of the qubit. This is because the CZ gate will only have an effect if the qubit state has a nonzero amplitude in the $|1\rangle$ state. Thus, there will be no effect if the qubit is in state $|0\rangle$, while if it is prepared in state $|+\rangle$, the scattering of the photon will flip the state to $|-\rangle$. The HADAMARD gates will be applied at each time bin following a reversed binary logic to flip the qubit state correspondingly. The reason for the choice of using reversed binary logic for the encoding is that

$$\sum_{n=0}^{2^m-1} |[\bar{n}]_2\rangle_A |[\bar{n}]_2\rangle_B = (|0_A 0_B\rangle + |1_A 1_B\rangle)^{\otimes m}, \quad (2)$$

where $[\bar{i}]_2$ is the inverse of the binary formation of i in digit size m , for example, when $m = 3$, $[0]_2 \rightarrow 000$, $[\bar{1}]_2 \rightarrow 100$, $[\bar{2}]_2 \rightarrow 010$, $[\bar{3}]_2 \rightarrow 110$, etc. The reversed binary logic thus ensures compatibility with the conventional bit ordering of the register qubits. We note that this choice is, however, arbitrary and standard binary encoding could also be used.

Second, we circumvent the use of optical switches in the final photonic X measurement by replacing the switches with passive beam splitters and delay loops. This results in a nonzero, heralded failure probability of the measurement. Nonetheless, the success probability can be boosted through a concatenated array of beam splitters and delay lines.

We now go through the steps of the protocol in more detail. First, Alice generates a time-bin photonic qudit with dimension 2^m , where m is the number of entangled pairs we want to generate. We model this generation assuming a cavity-assisted Raman scheme similar to the approach in Ref. [22].

We consider a three-level system consisting of two stable ground states $|g_0\rangle, |g_1\rangle$ and one excited state $|e_1\rangle$. The transition $|e_1\rangle \leftrightarrow |g_1\rangle$ is coupled to an optical cavity for efficient photon extraction, while the transition $|e_1\rangle \leftrightarrow |g_0\rangle$ is driven by a pulsed laser.

The system is initialized in state $|g_0\rangle$. At each time bin, we drive with pulsed excitation such that there is a small probability that the system is transferred from the ground state $|g_0\rangle$ to $|g_1\rangle$ with the emission of a cavity photon. By carefully tuning the amplitude of the driving pulses, a time-bin encoded photonic qudit of the following form will be emitted in the ideal case:

$$|\psi\rangle_{ph} = \sum_{n=0}^{2^m-1} \alpha_n |n\rangle_{ph}, \quad (3)$$

where $|n\rangle_{ph}$ denotes a single photon in the n th time bin and vacuum in the rest.

The amplitudes $\alpha_n \in \mathbb{R}^+$ can be tuned through the amplitude of the driving pulses. This becomes important later on as the probabilistic time-bin erasure step at the end of the entanglement generation protocol will affect the amplitude of the time bins differently. This, as well as the general asymmetric loss in the setup, can be compensated by tuning the initial amplitudes. We discuss the exact form of α_n below.

Next, the generated photonic qudit interacts with the qubits in Alice's register. This interaction ensures that the photonic

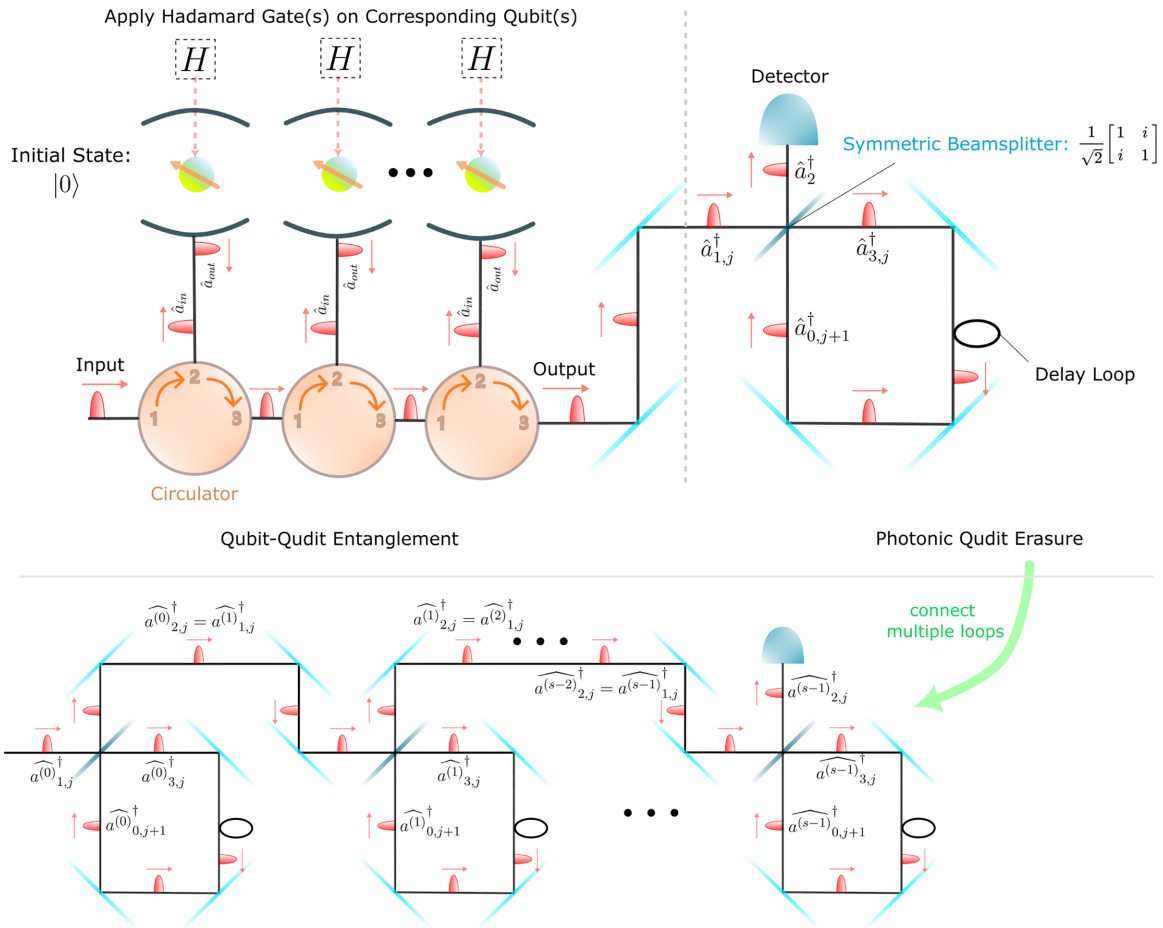


FIG. 2. The main elements of the switch-free qudit-mediated entangling protocol. On the top left, we show the qubit-qudit entangling operation that Alice and Bob perform. The initial states of the qubits are $|0\rangle$ and HADAMARD gates are applied to specific qubits at each time bin to ensure the correct qudit-qubit interactions. On the top right, we show the final measurement of the photon, which erases the time-bin information and heralds successful entanglement generation. Upon arrival at the symmetric beam splitter, the photon is either reflected and detected or transmitted and delayed by exactly one time bin. To boost the probability of a successful time-bin erasure, a concatenated series of beam splitters and delay loops can be used, as illustrated at the bottom of the figure.

qudit is entangled with the qubits. The register qubits of Alice and Bob are all initialized in state $|0\rangle$. Each time-bin pulse will interact with all register qubits through a cavity-mediated CZ gate [23,24]. This interaction ensures reflection of the photon from the cavity-spin system with (without) a π phase shift if the spin is in an uncoupled (coupled) state to the cavity.

Suppose that the spin state is $\alpha|0\rangle + \beta|1\rangle$, where only state $|1\rangle$ is coupled to an excited state via the cavity field. Reflecting a single photon in the first time bin ($|0\rangle_{ph}$) will result in the transformation $|0\rangle_{ph} \otimes (\alpha|0\rangle + \beta|1\rangle) \rightarrow |0\rangle_{ph} \otimes (\alpha r_0|0\rangle + \beta r_1|1\rangle)$. Ideally, $r_0 = -1$ and $r_1 = 1$, which corresponds to a perfect CZ gate up to a global phase.

We can control whether the scattering of a photon will flip the state of a qubit through the application of HADAMARD gates. This is done according to a reversed binary encoding of the time-bin number. As an example, we consider the case of $m = 3$. Starting from the initial state $\sum_{n=0}^7 \alpha_n |n\rangle_{ph} |000\rangle$, the procedure would be as follows:

- (a) At time bin $|0\rangle_{ph}$:
 - (1) No HADAMARD gates applied
 - (2) First time-bin pulse is reflected

- (b) At time bin $|1\rangle_{ph}$:
 - (1) Apply HADAMARD on the first qubit
 - (2) Second time-bin pulse is reflected

Resulting state: $-\alpha_0 |0\rangle_{ph} |000\rangle + \sum_{n=1}^7 \alpha_n |n\rangle_{ph} |000\rangle$

- (c) At time bin $|2\rangle_{ph}$:
 - (1) Apply HADAMARD on the second qubit
 - (2) Third time-bin pulse is reflected

Resulting state: $-\alpha_0 |0\rangle_{ph} |000\rangle - \alpha_1 |1\rangle_{ph} |100\rangle + \sum_{n=2}^7 \alpha_n |n\rangle_{ph} |000\rangle$

- (d) At time bin $|3\rangle_{ph}$:
 - (1) Apply HADAMARD on the first two qubits

(2) Fourth time-bin pulse is reflected

$$|3\rangle_{ph}|++0\rangle \rightarrow -|3\rangle_{ph}|--0\rangle$$

(3) Apply HADAMARD on the first two qubits

Resulting state:

$$-\alpha_0|0\rangle_{ph}|000\rangle - \alpha_1|1\rangle_{ph}|100\rangle - \alpha_2|2\rangle_{ph}|010\rangle$$

$$-\alpha_3|3\rangle_{ph}|110\rangle + \sum_{n=4}^7 \alpha_n|n\rangle_{ph}|000\rangle$$

(e) . . .

Repeating this process for all time bins, Alice's register qubits will be entangled with the photonic qudit in the following way:

$$\begin{aligned} |\psi\rangle = & \alpha_0|0\rangle_{ph}|000\rangle + \alpha_1|1\rangle_{ph}|100\rangle \\ & + \alpha_2|2\rangle_{ph}|010\rangle + \alpha_3|3\rangle_{ph}|110\rangle \\ & + \alpha_4|4\rangle_{ph}|001\rangle + \alpha_5|5\rangle_{ph}|101\rangle \\ & + \alpha_6|6\rangle_{ph}|011\rangle + \alpha_7|7\rangle_{ph}|111\rangle, \end{aligned} \quad (4)$$

after the scattering of the final (eighth) time bin up to a global phase. This can be straightforwardly extended to general m . Bob will perform the same procedure upon receiving the transmitted qudit from Alice.

After the scattering of the final time bin at Bob's side, the total state of the qudit and Alice and Bob's register qubits will be

$$|\psi\rangle = \sum_{n=0}^{2^m-1} \alpha_n |n\rangle_{ph} |[\bar{n}]_2\rangle_A |[\bar{n}]_2\rangle_B. \quad (5)$$

Next, we need to unentangle the qudit from the spin qubits by measuring the qudit in a manner that erases the time-bin information. By measuring the photon, we also herald that the protocol was successful.

A single-loop, switch-free photon measurement approach is shown at the top right of Fig. 2. A symmetric beam splitter will either transmit a time-bin pulse into a delay loop or reflect it to a single-photon detector. The delay is tuned such that a delayed time bin will interfere with the successive time bin at the beam splitter.

To see how this can erase the time-bin information, we consider an example with only two time bins. In this case, a detection at a time corresponding to the second time bin will erase the information about whether the photon was initially in the first or second time bin. Note, however, that the process is probabilistic since a detection at the first time bin determines that the photon was initially in the first time bin.

This can be extended to interfering all time bins through careful tuning of the initial qudit amplitudes, as we will show later. However, since the photon erasure is probabilistic, we can also connect multiple photon loops to increase the measurement success probability, as shown in the bottom of Fig. 2. Nevertheless, the connected delay loops lead to several interference effects not present in the single-loop case:

(i) Destructive interference. We find that due to destructive interference, certain detection times later than the 2^m -th time bin will not project into a superposition of 2^m spin states, but only a subset of these.

(ii) The tuning of α_n depends on the specific detection time and number of loops. For the single loop, the tuning of the coefficients α_n does not depend on the exact detection time as

long as this is later than, or at, the 2^m -th time bin. However, in the connected loops, this is not the case.

(iii) Phase correction problem. For the single loop, the phase due to the beam-splitter transformation can always be corrected by single-qubit gates. For the connected loops, this is not always the case, depending on the specific detection time and the number of loops.

We will now go through these setups in more detail and also refer the reader to Appendix A 3 for additional information. For a setup with $s \geq 1$ delay loops and a detection time of $u \geq 2^m$ (in units of the time-bin duration), we define

$$Y(s, u, n) = \sum_{t=1}^{\min[s, u-n]} (-1)^{t+1} \binom{s}{t} \binom{u-n-1}{t-1}. \quad (6)$$

One has to choose s and u such that $Y(s, u, n)$ have the same sign throughout all n , i.e.,

$$\begin{aligned} Y(s, u, n) > 0 \text{ or } Y(s, u, n) < 0 \\ \text{for } \forall n \in \{0, 1, 2, \dots, 2^m - 1\}, \end{aligned} \quad (7)$$

to ensure that we can find suitable coefficients α_n such that the final qubit state following the photon detection is equivalent to m copies of the Bell state $|\Phi^+\rangle = (|0_A 0_B\rangle + |1_A 1_B\rangle)/\sqrt{2}$ up to single-qubit gate corrections. The tuning of the coefficients is determined by

$$\alpha_n^2 = \left(\sum_{k=0}^{2^m-1} 2^{n-k} \left| \frac{Y(s, u, n)}{Y(s, u, k)} \right|^2 \right)^{-1}. \quad (8)$$

In this way, after the successful photon detection, we have the state

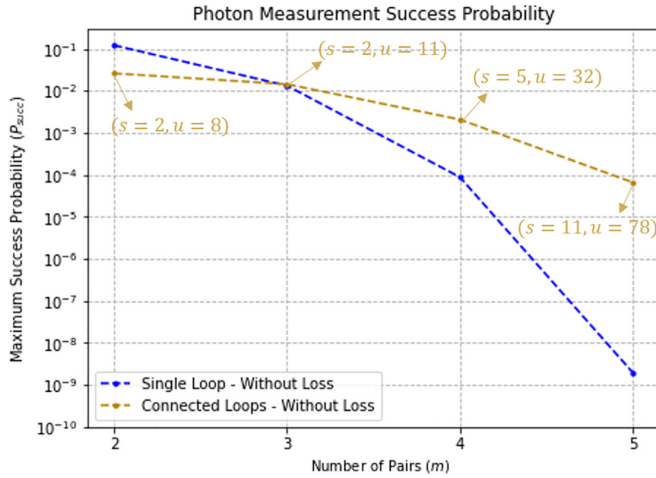
$$|\psi\rangle = \frac{1}{2^{\frac{m}{2}}} \bigotimes_{n=0}^{m-1} (|0_A 0_B\rangle + i^{-2^n} |1_A 1_B\rangle), \quad (9)$$

where the extra phase i^{-2^n} can be easily corrected by applying single-qubit gates. The probability to detect the photon at time u is

$$P_{\text{succ}}(s, u, m) = 2^m \left(\sum_{k=0}^{2^m-1} 2^{s+u-k} \left| \frac{1}{Y(s, u, k)} \right|^2 \right)^{-1}. \quad (10)$$

It is important to note that in the single-loop case of $s = 1$, there are no interference effects and measuring every time bin after time bin $2^m - 1$ leads to success. Therefore, one can find that in this case, the measurement always succeeds when $u \geq 2^m$, and the success probability for the single-loop scenario should be the sum over all $P_{\text{succ}}(s = 1, m, u \geq 2^m)$.

To illustrate the increase in probability by connecting more loops, we have plotted the success probabilities of measurements under both single loops and interconnected loops in Fig. 3. In this plot, we demonstrate that connecting loops can substantially enhance the success probability, especially for a larger number of Bell pairs, despite the fact that in the single-loop cases, all instances where $u \geq 2^m$ can be considered as successful. We note that we have not included loss in the optical elements and delay lines so far. We will discuss the effect of this in the following section. We also refer the reader to Fig. 9 in Appendix A 3 for a version of Fig. 3 with loss included.



s (# loops) range for connected loops: 2~15
 u (# clicking time) range for connected loops: $2^m \sim 2^m + 50$

FIG. 3. The photon measurement success probability for a single loop and concatenated loops. For the single loop, the success probability is the sum over all $P_{\text{succ}}(s = 1, m, u \geq 2^m)$. For the connected loops, the success probability shown here is the maximum probability within the ranges of (s, u) shown above. The optimal (s, u) for each number of entangled pairs is marked on the plot.

III. ERROR ANALYSIS AND ERROR CORRELATIONS

So far, we have not considered the effect of noise and general experimental imperfections. These will affect both the success probability of the protocol and the fidelity of the generated Bell pairs. To analyze this, we model the effect of the following possible imperfections on our protocol: (1) imperfections in the generation of the photonic qudit due to phase and amplitude fluctuations of the laser drive, (2) dephasing of the photonic qudit due to phase instability of the optical circuit including the photonic X-basis measurement, (3) imperfect cavity scattering in the spin-photon CZ gate, (4) single-qubit gate errors, (5) spin qubit decoherence, and (6) photon losses. We model both phase fluctuations of the laser drive and the general dephasing from optical instability as random varying phases of the time-bin pulses as discussed in Appendix A 1.

Photon loss is different from the other imperfections as we herald the detection of a photon. In our analysis, we assume that dark counts are negligible and the loss is accurately characterized such that we can compensate for the effect on the fidelity of the generated entanglement by tuning the initial amplitudes of the photonic qudit (see Appendix A 3 for details). Photon loss will therefore only affect the success probability of the protocol.

The other imperfections will decrease the fidelity of the generated Bell pairs since they are not heralded. Moreover, they can lead to correlated errors, which means that some errors may be propagated to multiple generated Bell pairs. This can occur since all register qubits are entangled with one single photon and any imperfections of the photon and operations may lead to correlated errors. The details of our error modeling are presented in Appendix A. The decrease in

the average fidelity of the generated Bell pairs is shown in Fig. 4(a) for a specific range of error parameters.

To quantify the amount of error correlation between the Bell pairs, we use the following approach. Suppose the probabilities that a Pauli error happens on qubits a and b are $\epsilon_a (\ll 1)$ and $\epsilon_b (\ll 1)$, respectively, while the probability that a Pauli error happens on both qubits a and b is ϵ_{ab} . If $\epsilon_{ab} = \epsilon_a \epsilon_b$, the errors on qubits a and b are independent and we call them “uncorrelated” throughout this paper, while if $\epsilon_{ab} \neq \epsilon_a \epsilon_b$ holds, the errors are dependent and we refer to them as “correlated” errors.

In general, an independent error model is of the form

$$\rho_{\text{uncorrelated}} = \Lambda_{2m}[\dots(\Lambda_3\{\Lambda_2[\Lambda_1(\rho_{\text{perfect}})]\})], \quad (11)$$

where Λ denotes the corresponding Pauli error channel (I, X, Y, Z) on each register qubit ($2m$ in total). In this case, multiqubit errors happen with very low probability since $\epsilon_{ab} \ll \epsilon_a, \epsilon_b$. However, if $\epsilon_{ab} \neq \epsilon_a \epsilon_b$, the errors among the pairs are correlated. We quantify the amount of error correlations for the qudit-mediated entanglement generation in the following way.

Let $\rho_{\text{correlated}}$ be the output density matrix of the qubits after a successful entanglement generation of the qudit protocol for a specific choice of error parameters. The fidelity between this state and the perfect output state (collection of m Bell pairs) is denoted by $F(\rho_{\text{correlated}})$. Similarly, the fidelity between the perfect state and the output of the uncorrelated error channel in (11) is $F(\rho_{\text{uncorrelated}})$. We then let $T_{\min} = \min_{\Lambda} T(\rho_{\text{uncorrelated}}, \rho_{\text{correlated}})$ such that $|F(\rho_{\text{correlated}}) - F(\rho_{\text{uncorrelated}})| \leq \epsilon$ for sufficiently low ϵ (we choose $\epsilon = 10^{-4}$ in this work) quantify how large the error correlation is.

Figure 4(b) shows how the amount of error correlations in the qudit protocol increases as the general errors increase. Furthermore, we see how the amount of correlation increases with the number of pairs. In the following two sections, we consider two strategies for mitigating the effect of the errors and obtain high-fidelity Bell pairs: entanglement purification and quantum error correction.

IV. PURIFICATION PERFORMANCE

Entanglement purification is a method that aims to produce one (or possibly more) high-fidelity entangled pair(s) from a collection of noisy pairs [9,10,15,25]. It is a key element to reducing noise in first-generation quantum repeaters [26].

To search for optimal purification protocols, we use the evolutionary algorithm from Ref. [17], which enables m -to-one purification for any number of generated noisy Bell pairs, m . Note that in this work, we adapt the original protocol in Ref. [17] to a single-round scheme, which only uses simultaneously generated Bell pairs, instead of repeating the purification for many rounds with fewer pairs. Therefore, when multiple pairs are successfully generated simultaneously, we find the optimal local operations and classical communication (LOCCs) on all $2m$ local registers that output one higher-fidelity entangled pair, with the other $m - 1$ pairs measured out eventually. For the details of the purification protocol that we implement in our work, we refer the reader to Appendix B. The performance of the optimized purification

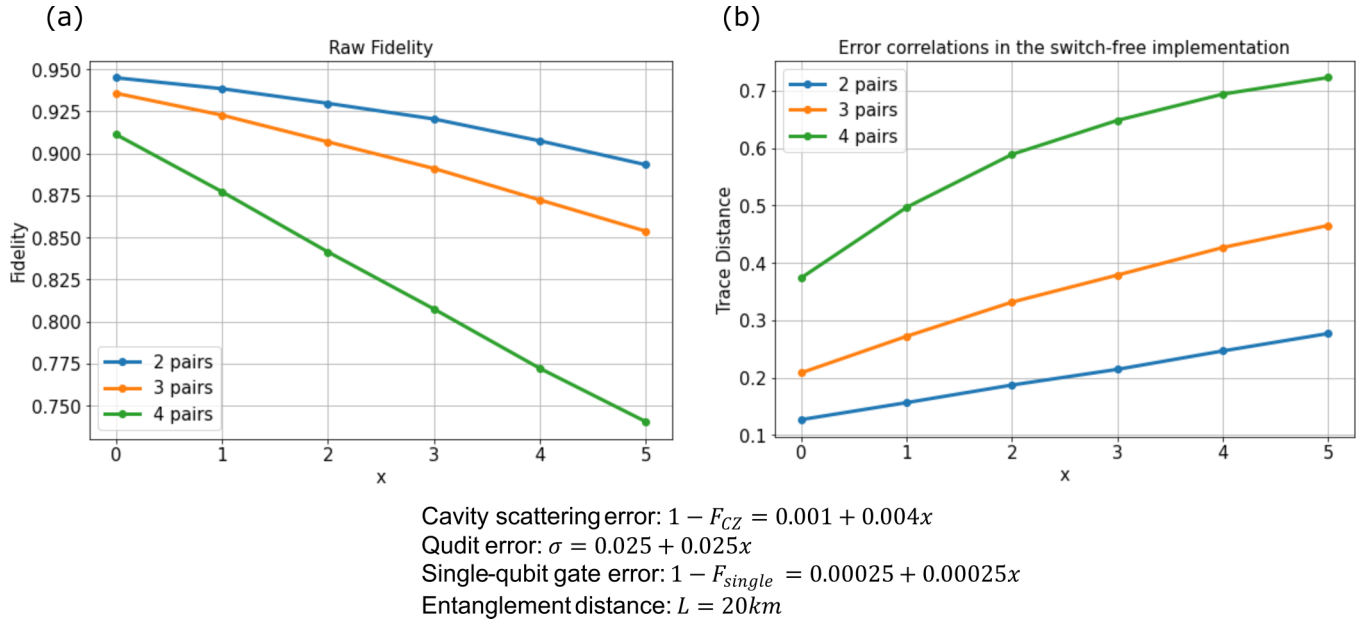


FIG. 4. (a) Raw fidelity of the generated Bell pairs using the switch-free qudit protocol. (b) Error correlations under the specified error environment. One can notice that in (a) and (b), the raw fidelity will decrease and the error correlations will grow when increasing errors and the number of generated pairs.

circuits is shown in Figs. 5(a) and 5(b). We see that the purification protocol successfully produces a higher-fidelity entangled pair from the collection of noisy pairs.

We also investigate how well this optimized purification protocol can mitigate the error correlations. For each error data point, we find the matching uncorrelated error channel following the approach outlined in Sec. III. We find the optimal purification protocol for the uncorrelated error channel and compare it with the performance of the optimized purification of the qudit-mediated entangled state. The result is shown in Fig. 5(a). We see that for the purification of a few pairs, the purification of the qudit-mediated entanglement performs slightly worse. However, the performance difference decreases as the number of pairs increases since the

purification circuit has more freedom to target the dominant error terms. Thus, it seems that optimizing the purification circuit allows one to target the dominant errors regardless of whether or not they are correlated. Note that we assume perfect operations in the purification circuit in Figs. 5(a) and 5(b) to focus on the ability to target the errors from the entanglement generation procedure.

V. TELEPORTATION-BASED QUANTUM ERROR CORRECTION

Teleportation-based quantum error correction is another method to correct for noisy connections in a quantum network, as exploited in so-called second-generation quantum

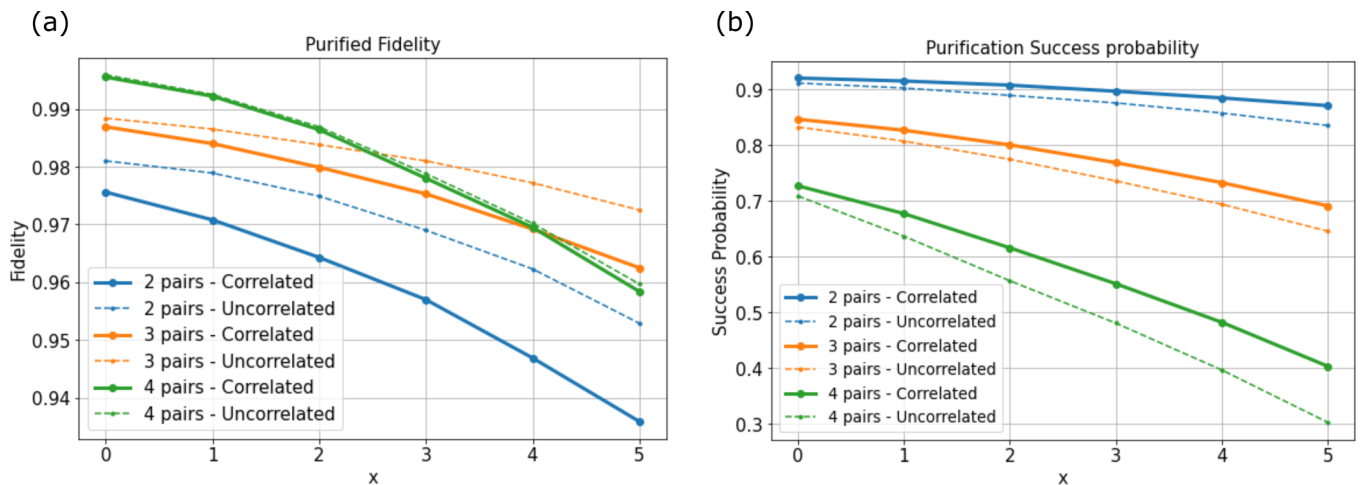


FIG. 5. (a) Purified fidelity for error-correlated and error-uncorrelated pairs, and (b) purification success probability under the specified error environment shown below. The error range is the same as in Fig. 4. For the purification plots (a) and (b), one can see an obvious fidelity increase after the purification [the raw pair fidelity has been shown in Fig. 4(a)]. The error range shown in the plot is the same as in Fig. 4.

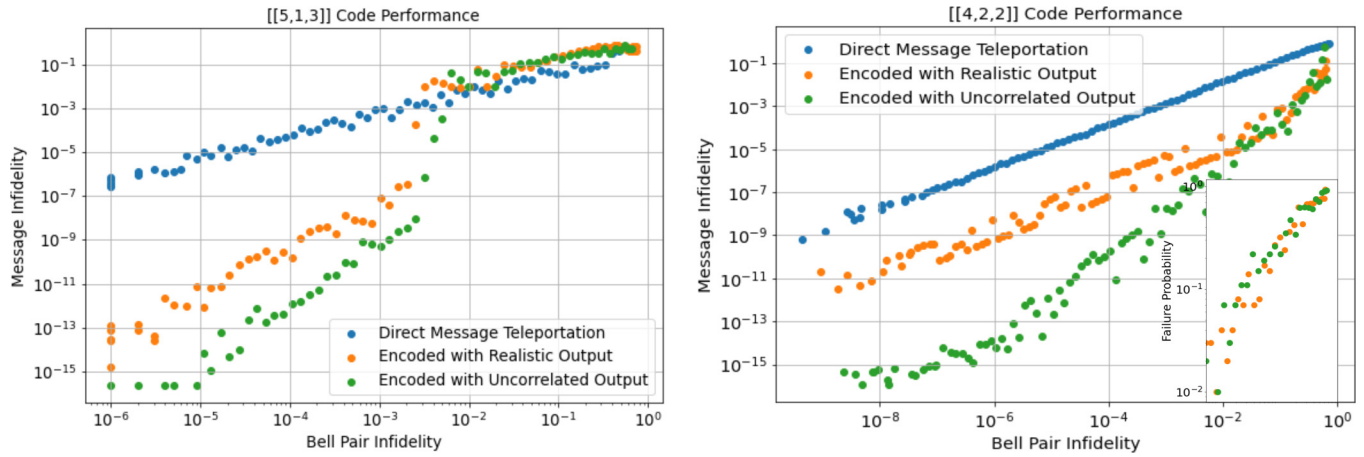


FIG. 6. The performance of teleportation-based $[[5,1,3]]$ and $[[4,2,2]]$ codes under the switch-free implementation. For each code, we simulate the infidelity of the transmitted message against the Bell pair infidelity. The blue dots correspond to direct message teleportation, i.e., without encoding and using a single Bell pair. The orange and green dots correspond to the correction code, teleported by multiple Bell pairs with correlated (output from the realistic correlated error model of the switch-free qudit protocol) and uncorrelated error models, respectively. The $[[4,2,2]]$ code can only detect and not correct errors; thus we also show the probability that the code fails to detect an error in the inset on the right. Here, we assume perfect encoding and decoding operations.

repeaters [11,12,26] and modular quantum computing [27]. In the teleportation-based setting, Alice wishes to teleport an encoded message to Bob via multiqubit quantum teleportation [28,29] requiring the simultaneous availability of multiple entangled pairs [18–21].

We consider two simple codes: the $[[5,1,3]]$ and the $[[4,2,2]]$ codes requiring five and four Bell pairs, respectively, for teleportation. The former is the smallest code that can perform quantum error correction [30], and the latter only detects the errors due to its limited code space [31]. The Bell pairs are generated with the qudit protocol and we assume perfect operations in the encoding and decoding of the message to focus on the ability of the code to correct errors from the noisy Bell pairs.

The simulation results are shown in Fig. 6, where we compare the fidelity of the encoded transmission to the fidelity of teleporting unencoded qubits. We sample the qubit states (one-qubit teleportation for the $[[5,1,3]]$ code and two-qubit teleportation for the $[[4,2,2]]$ code) to be teleported at random, and each data point denotes the average result over all sampled random cases. Notably, for the $[[5,1,3]]$ code, there is a threshold above which the encoding performs worse than the unencoded transmission. We find the threshold around a Bell pair infidelity of $\sim 10^{-3}$. Such a threshold is always found for quantum error correcting codes since, for high enough error rates, the error correction process adds more errors than it removes. Thus, above this threshold, the net total error increases. For the $[[4,2,2]]$ code, however, we see that teleporting the perfect code will always win if we only consider the transmitted message fidelity. However, since the $[[4,2,2]]$ code cannot correct the errors but only detect them, the transmitted message will fail if an error is detected, resulting in a nondeterministic transfer.

We also investigate the effect of correlated errors on the performance of the error correction, following the same approach as for entanglement purification. We see from Fig. 6 that the codes perform worse on the error-correlated states.

In contrast to the purification circuit, these codes are also not designed for correlated errors, which might be a subject for further study.

VI. CONCLUSION AND DISCUSSION

In this paper, we have proposed a different implementation of a qudit-mediated entanglement generation protocol that completely circumvents the use of optical switches. Notably, we show how probabilistic erasure of the photon time-bin information can be implemented with passive linear optics elements and how the success probability can be increased through the concatenation of beam splitters and delay loops.

In previous protocols, the use of optical switches allows, in principle, for a deterministic operation, in contrast to the scheme considered here. In practice, fast optical switches tend to be lossier than beam splitters, which can have close to negligible losses. In Ref. [13], the photon erasure includes $2^m - 1$ fast optical switches, and $2^{m-1}(2^m - 1)$ delay lines. Forgetting about the experimental difficulty in operating such a large optical circuit, we can estimate how efficient the optical switches need to be to surpass the efficiency of the probabilistic scheme. To generate m Bell pairs, the photonic qudit in Ref. [13] goes through an average of m switches. To reach the same success probability as in Fig. 10, the efficiency of the switches should be $\sim 20\text{--}30\%$.

In addition, we have simulated the amount of error correlation that the qudit protocol introduces between the simultaneously generated Bell pairs and its impact on key applications such as entanglement purification and quantum error correction. We found that significant error correlations are introduced, but through optimization of the purification circuit [17], the errors can still be efficiently targeted. For the two quantum error correcting codes, the $[[5,1,3]]$ and $[[4,2,2]]$ codes that we considered for teleportation negatively impact the performance.

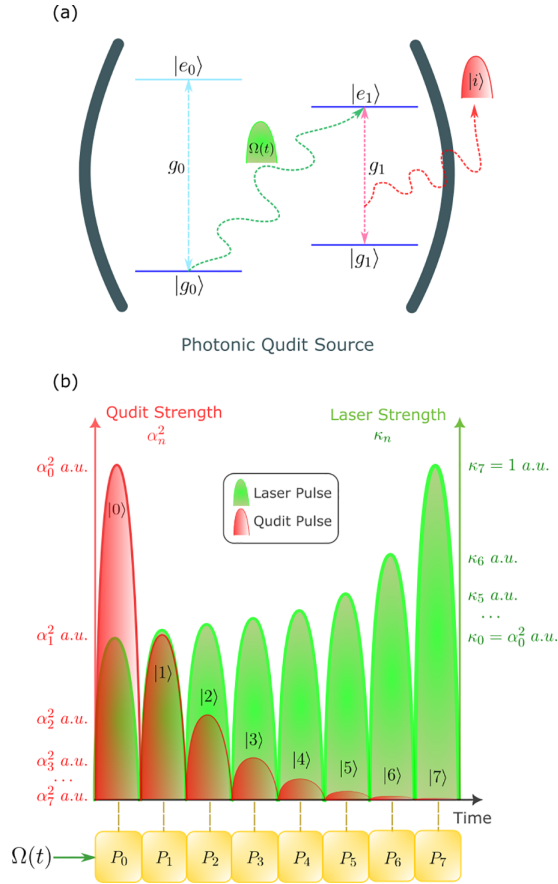


FIG. 7. (a) Schematic of the photonic qudit. The laser pulses drive a cavity-assisted Raman transition from the initial state $|g_0\rangle$ to $|g_1\rangle$ with the emission of a photon. (b) Example of how varying the amplitude of the laser pulses affects the amplitude of the resulting qudit state.

Given the significantly reduced memory requirements for the spin qubits [13], this protocol can be used to boost the performance of current quantum hardware for quantum networking. In particular, quantum repeaters, where the distillation of high-fidelity Bell pairs through entanglement purification is a key requisite, necessitate the availability of multiple Bell pairs at the same point in time. Importantly, we have shown that high-fidelity entanglement can indeed be distilled from the simultaneously generated Bell pairs in the qudit protocol, even in the presence of correlated errors.

ACKNOWLEDGMENTS

We thank Yunzhe Zheng (TUDelft) and Hemant Sharma (TUDelft) for the supportive discussions about the qudit-mediated entanglement distributions and cavity scatterings. We thank Stefan Krastanov (UMass Amherst) for the useful comments and inputs on the genetically optimized purification protocol. We acknowledge funding from the NWO Gravitation Program Quantum Software Consortium (Project QSC No. 024.003.037). J.B. acknowledges support from The AWS Quantum Discovery Fund at the Harvard Quantum Initiative. L.M. partly carried out her work in the framework of the Russian Quantum Technologies Roadmap. L.M.

was supported by the Netherlands Organisation for Scientific Research (NWO/OCW), as part of the Quantum Software Consortium program (Project QSC No. 024.003.037/3368).

APPENDIX A: ERROR MODELS

Here we discuss the analytical error estimations for the switch-free, qudit-mediated entanglement generation protocol.

1. Photonic qudit generation and imperfections

At the beginning of the switch-free implementation, Alice should generate a photonic time-bin qudit with 2^m pulses. We consider a Raman scheme for photonic qudit generation, which has been experimentally realized in quantum dot [32] and silicon-vacancy diamond systems [22]. The setup is shown in Fig. 7(a). We initialize the emitter in state $|g_0\rangle$. At each time bin, a laser pulse drives with a tunable probability the transition from $|g_0\rangle$ to $|g_1\rangle$ with the emission of a cavity photon.

Here, we illustrate an example. Suppose we would like to generate an eight-time-bin photonic qudit illustrated in Eq. (3) (where $m = 3$) as follows:

(a) At time bin $|0\rangle_{ph}$, the pulse P_0 drives $|g_0\rangle$ to $|g_1\rangle$ with the emission of $|0\rangle_{ph}$ resulting in the state

$$|g_0\rangle \rightarrow \sqrt{1 - \alpha_0^2} |g_0\rangle |\text{vac}\rangle_{ph} + \alpha_0 |g_1\rangle |0\rangle_{ph}. \quad (\text{A1})$$

(b) At time bin $|1\rangle_{ph}$, the pulse P_1 drives again $|g_0\rangle$ to $|g_1\rangle$ with the emission of $|1\rangle_{ph}$ such that

$$\begin{aligned} & \sqrt{1 - \alpha_0^2} |g_0\rangle |\text{vac}\rangle_{ph} + \alpha_0 |g_1\rangle |0\rangle_{ph} \\ & \rightarrow \sqrt{1 - \alpha_0^2 - \alpha_1^2} |g_0\rangle |\text{vac}\rangle_{ph} + |g_1\rangle (\alpha_0 |0\rangle_{ph} + \alpha_1 |1\rangle_{ph}). \end{aligned} \quad (\text{A2})$$

(c) At time bin $|2\rangle_{ph}$, the pulse P_2 drives $|g_0\rangle$ to $|g_1\rangle$ with the emission of $|2\rangle_{ph}$ such that

$$\begin{aligned} & \sqrt{1 - \alpha_0^2 - \alpha_1^2} |g_0\rangle |\text{vac}\rangle_{ph} + |g_1\rangle \sum_{n=0}^1 \alpha_n |n\rangle_{ph} \\ & \rightarrow \sqrt{1 - \left(\sum_{n=0}^2 \alpha_n^2 \right)} |g_0\rangle |\text{vac}\rangle_{ph} + |g_1\rangle \sum_{n=0}^2 \alpha_n |n\rangle_{ph}. \end{aligned} \quad (\text{A3})$$

(d) . . .

Continuing the procedures until the final time bin $|7\rangle_{ph}$, we will have removed all the amplitude of the $|g_0\rangle$ state such that the emitter is in state $|g_1\rangle$ and the photonic state is

$$|\psi\rangle_{ph} = \sum_{i=0}^7 \alpha_i |i\rangle_{ph}, \quad (\text{A4})$$

where $\sum_{n=0}^{2^m-1} \alpha_n^2 = 1$. This procedure can readily be extended to any qudit dimension.

Note that at each time bin, different laser driving strengths should be applied to generate each time-bin pulse, as shown in

Fig. 7(b). For example, as shown for the eight-time-bin case in Fig. 7, $P_0 = \alpha_0^2$, $P_1 = \frac{\alpha_1^2}{1-\alpha_0^2}$, $P_2 = \frac{\alpha_2^2}{1-\alpha_0^2-\alpha_1^2}$, ..., $P_7 = \frac{\alpha_7^2}{1-\sum_{k=0}^6 \alpha_k^2}$. For a general 2^m -time-bin case, we have

$$P_0 = \alpha_0^2 \quad (\text{A5})$$

and

$$P_n = \frac{\alpha_n^2}{1 - \sum_{k=0}^{n-1} \alpha_k^2} \text{ for } 1 \leq n \leq 2^m - 1. \quad (\text{A6})$$

Imperfect cavity coupling will predominantly lead to loss of the photon or dephasing of the qudit state through spontaneous decay from the excited state $|e_1\rangle$ followed by re-emission. The first can be absorbed in the general transmission probability of the photon in the scheme. In addition, phase and amplitude fluctuations of the laser drive can also lead to dephasing and modulation of the amplitudes of the desired qudit state in addition to dephasing of the spin states. Moreover, since different time bins experience different amounts of delay, the phase instabilities will also lead to an overall dephasing of the qudit state and therefore we absorb this imperfection as an overall dephasing channel to the photonic qudit, along with the laser drive noise.

All the errors considered above lead to dephasing and modulation of the amplitudes of the desired qudit state. We choose a simplified model where we model these imperfections as random Gaussian fluctuations applied to the laser drive since this will lead to the same effect. The output qudit state is thus modeled as

$$\begin{aligned} |\psi\rangle_{ph} &= \sum_{n=0}^{2^m-1} \sqrt{1 + \frac{\zeta_n}{P_n} \alpha_n e^{i\theta_n}} |n\rangle_{ph} \\ &\approx \sum_{n=0}^{2^m-1} \left(1 + \frac{\zeta_n}{2P_n}\right) \alpha_n e^{i\theta_n} |n\rangle_{ph}. \end{aligned} \quad (\text{A7})$$

For simplicity, we consider $\theta_n \sim N(0, \sigma^2)$ and $\zeta_n \sim N(0, \frac{1}{\sum_{k=0}^{2^m-1} \alpha_k^4 P_k^{-2}} \sigma^2)$. This is to make sure that the total amplitude error gives $\sum_{n=0}^{2^m-1} \frac{\alpha_n^2}{P_n} \zeta_n \sim N(0, \sigma^2)$.

2. Cavity scattering

In the main text, we discussed that after scattering of a photon, the qubit state $\alpha|0\rangle + \beta|1\rangle$ will become $\alpha r_0|0\rangle + \beta r_1|1\rangle$ and, ideally, $r_0 \approx -1$ and $r_1 \approx 1$, which forms a perfect CONTROL-Z gate. In the nonideal case, however, one may consider the four-level cavity system with two ground states $|0\rangle$, $|1\rangle$ and their excited states $|e_0\rangle$, $|e_1\rangle$ shown in Fig. 8 [13,33–35], as this is a good model for realistic hardware such as quantum dots and group-IV diamond vacancy systems.

Here, we briefly introduce the model used in this work. One may refer to Ref. [13] for more details. We denote \hat{c} as the annihilation operator of the cavity field and Δ_0 (Δ_1) as the detuning between the transitions $|0\rangle \leftrightarrow |e_0\rangle$ ($|1\rangle \leftrightarrow |e_1\rangle$) and the cavity mode. The coupling rate of the two transitions is g_0 and g_1 , respectively. The Hamiltonian H of the system is

$$\begin{aligned} H &= \Delta_0 |e_0\rangle \langle e_0| + \Delta_1 |e_1\rangle \langle e_1| \\ &+ (g_0 |e_0\rangle \langle 0| \hat{c} + \text{h.c.}) + (g_1 |e_1\rangle \langle 1| \hat{c} + \text{H.c.}). \end{aligned} \quad (\text{A8})$$

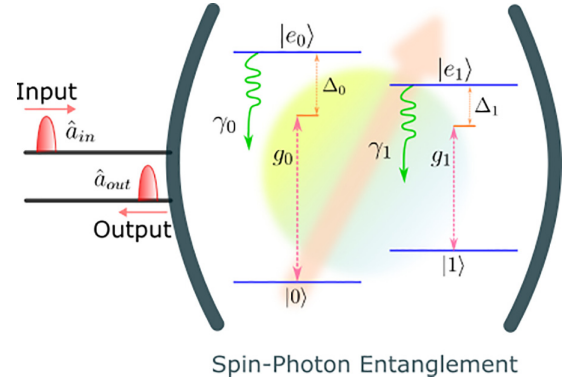


FIG. 8. The structure of a spin-photon entanglement system in a four-level cavity [13,33–35]. \hat{a}_{in} and \hat{a}_{out} are the photonic input and output of the cavity system, respectively. $|e_0\rangle$ and $|e_1\rangle$ denote the corresponding excited states of $|0\rangle$ and $|1\rangle$. g_0 and g_1 are the transition couplings. Δ_0 and Δ_1 are the detunings between the transition coupling and the cavity mode. γ_0 and γ_1 denote the spontaneous emissions of $e_0 \rightarrow |0\rangle$ and $e_1 \rightarrow |1\rangle$, respectively.

Considering the spin-photon interaction in the weak-driving regime, one can derive the reflection coefficients r_0 (r_1) for the state $|0\rangle$ ($|1\rangle$),

$$\begin{aligned} r_0 &= 1 - \frac{K_{in}/K}{-\frac{i\omega}{K} + \frac{1}{2} + \frac{C_0}{-\frac{i}{\gamma_0}(\omega + \Delta_0) + \frac{1}{2}}}, \\ r_1 &= 1 - \frac{K_{in}/K}{-\frac{i\omega}{K} + \frac{1}{2} + \frac{C_1}{-\frac{i}{\gamma_1}(\omega + \Delta_1) + \frac{1}{2}}}, \end{aligned} \quad (\text{A9})$$

where K_{in} is the decay rate of the cavity field into the collected mode and K_{loss} is the cavity loss rate. Thus, the total cavity decay rate is $K = K_{in} + K_{loss}$. We also define the cooperativities C_0 and C_1 as

$$C_0 = \frac{|g_0|^2}{K\gamma_0}, \quad C_1 = \frac{|g_1|^2}{K\gamma_1}. \quad (\text{A10})$$

For example, if the atomic qubit state is in a perfect $|+\rangle = \frac{1}{\sqrt{2}}(|0\rangle + |1\rangle)$, after the cavity scattering, we get the following state (normalization omitted):

$$|n\rangle_{ph} \otimes \frac{1}{\sqrt{2}}(|0\rangle + |1\rangle) \xrightarrow{CS} |n\rangle_{ph} \otimes \frac{1}{\sqrt{2}}(r_0|0\rangle + r_1|1\rangle), \quad (\text{A11})$$

where $n \in [0, 2^m - 1]$. Ideally, $C \gg 1$ and $K_{in} \approx K$. Then we have

$$r_0 \approx -1, \quad r_1 \approx 1. \quad (\text{A12})$$

Therefore, in the ideal cases, this interaction will form a CONTROL-Z gate applying to the atomic qubit in the cavity.

3. Photon measurement

a. Single delay loop

We first calculate the case where there is one delay loop in the time-bin erasure. The right-hand side of Fig. 2(b) shows

an overview of this setup. We write the state (5) as follows:

$$\begin{aligned} |\psi\rangle &= \frac{1}{2^{\frac{m}{2}}} \sum_{n=0}^{2^m-1} \alpha_n |n\rangle_{ph} S_n \\ &= \frac{1}{2^{\frac{m}{2}}} \sum_{n=0}^{2^m-1} \hat{a}_{1,n}^\dagger |\text{vac}\rangle_{ph,n} \alpha_n S_n. \end{aligned} \quad (\text{A13})$$

Here, index n denotes the time bin and $S_n = |[\bar{n}]_2\rangle_A |[\bar{n}]_2\rangle_B$. We denote i as the imaginary unit. As shown in Fig. 2, the indices 0, 1, 2, and 3 denote the operator positions at the four ports of the symmetric beam splitter τ ,

$$\tau = \frac{1}{\sqrt{2}} \begin{bmatrix} 1 & i \\ i & 1 \end{bmatrix}. \quad (\text{A14})$$

Therefore, for the four ports of the symmetric beam splitter τ , we have

$$\begin{aligned} \hat{a}_{0,j}^\dagger &= \frac{1}{\sqrt{2}} (\hat{a}_{2,j}^\dagger + i\hat{a}_{3,j}^\dagger), \\ \hat{a}_{1,j}^\dagger &= \frac{1}{\sqrt{2}} (i\hat{a}_{2,j}^\dagger + \hat{a}_{3,j}^\dagger). \end{aligned} \quad (\text{A15})$$

Here, j denotes the time bin. The delay line between $\hat{a}_{3,j}^\dagger$ and $\hat{a}_{0,j+1}^\dagger$ moves a pulse in time bin j to time bin $j+1$. Ideally, this achieves $\hat{a}_{3,j}^\dagger \rightarrow \hat{a}_{0,j+1}^\dagger$. However, there can be

an additional probability of losing photons in the delay loop which will affect the amplitude of the pulses. We model this with a beam splitter with the following transfer matrix τ_η :

$$\tau_\eta = \frac{1}{\sqrt{2}} \begin{bmatrix} \sqrt{1-\eta} & \sqrt{\eta} \\ \sqrt{\eta} & -\sqrt{1-\eta} \end{bmatrix}, \quad (\text{A16})$$

where η is the probability to the lose a photon in the delay loop. Taking into account the lossy beam splitter, we find the following recurrence relations:

$$\hat{a}_{3,j}^\dagger = \sqrt{1-\eta} \hat{a}_{0,j+1}^\dagger + \sqrt{\eta} \hat{a}_{\text{lost}}^\dagger, \quad (\text{A17})$$

$$\hat{a}_{0,j}^\dagger = \frac{1}{\sqrt{2}} (\hat{a}_{2,j}^\dagger + i\sqrt{1-\eta} \hat{a}_{0,j+1}^\dagger + i\sqrt{\eta} \hat{a}_{\text{lost}}^\dagger). \quad (\text{A18})$$

For the operator going to the detector [denoted as \hat{a}_2^\dagger in Fig. 2(b)], we keep calculating the initial input operator $\hat{a}_{1,j}^\dagger$ denoted by \hat{a}_2^\dagger in different time bin n . Then we have

$$\begin{aligned} \hat{a}_{1,j}^\dagger &= \sum_{n \geq 1} \left(\frac{i^{n-1} (1-\eta)^{\frac{n}{2}}}{2^{\frac{n+1}{2}}} \hat{a}_{2,j+n}^\dagger + \frac{i^n \eta^{\frac{1}{2}} (1-\eta)^{\frac{n}{2}}}{2^{\frac{n+1}{2}}} \hat{a}_{\text{lost}}^\dagger \right) \\ &\quad + \frac{i\hat{a}_{2,j}^\dagger}{\sqrt{2}} + \frac{\sqrt{\eta} \hat{a}_{\text{lost}}^\dagger}{\sqrt{2}}. \end{aligned} \quad (\text{A19})$$

Since $\hat{a}_{1,j}^\dagger$ is carrying the qubit state S_j , one can calculate the final state as

$$\begin{aligned} |\psi\rangle &= \left(\frac{i}{2^{\frac{1}{2}}} \alpha_0 S_0 \right) |0\rangle_{ph} + \left(\frac{i}{2^{\frac{1}{2}}} \alpha_1 S_1 + \frac{(1-\eta)^{\frac{1}{2}}}{2} \alpha_0 S_0 \right) |1\rangle_{ph} + \left(\frac{i}{2^{\frac{1}{2}}} \alpha_2 S_2 + \frac{(1-\eta)^{\frac{1}{2}}}{2} \alpha_1 S_1 + \frac{i(1-\eta)}{2^{\frac{3}{2}}} \alpha_0 S_0 \right) |2\rangle_{ph} \\ &\quad + \left(\frac{i}{2^{\frac{1}{2}}} \alpha_3 S_3 + \frac{(1-\eta)^{\frac{1}{2}}}{2} \alpha_2 S_2 + \frac{i(1-\eta)}{2^{\frac{3}{2}}} \alpha_1 S_1 - \frac{(1-\eta)^{\frac{3}{2}}}{4} \alpha_0 S_0 \right) |3\rangle_{ph} + \dots + \\ &\quad + \left(\frac{i}{\sqrt{2}} \alpha_{x-1} S_{x-1} + \sum_{n=1}^{x-1} \frac{i^{n-1} (1-\eta)^{\frac{n}{2}}}{2^{\frac{n+1}{2}}} \alpha_{x-n-1} S_{x-n-1} \right) |x-1\rangle_{ph} + \left(\sum_{n=1}^x \frac{i^{n-1} (1-\eta)^{\frac{n}{2}}}{2^{\frac{n+1}{2}}} \alpha_{x-n} S_{x-n} \right) |x\rangle_{ph} \\ &\quad + \left(\sum_{n=1}^x \frac{i^n (1-\eta)^{\frac{n+1}{2}}}{2^{\frac{n+2}{2}}} \alpha_{x-n} S_{x-n} \right) |x+1\rangle_{ph} + \dots + \\ &\quad + \left(\sum_{n=1}^x \frac{i^{u+n-x-1} (1-\eta)^{\frac{u+n-x}{2}}}{2^{\frac{u+n-x+1}{2}}} \alpha_{x-n} S_{x-n} \right) |u\rangle_{ph} + \dots + (\text{loss terms}) \\ &= (\text{terms before } |x\rangle_{ph}) + \sum_{u=x}^{\infty} \frac{i^{u-x} (1-\eta)^{\frac{u-x}{2}}}{2^{\frac{u-x}{2}}} \left(\sum_{n=1}^x \frac{i^{n-1} (1-\eta)^{\frac{n}{2}}}{2^{\frac{n+1}{2}}} \alpha_{x-n} S_{x-n} \right) |u\rangle_{ph} + (\text{loss terms}), \end{aligned} \quad (\text{A20})$$

where we denote $x = 2^m$. Obviously, only when the detector clicks at or after time bin x , the final qubit states can be written in a nicely formed summation without information loss. In order to get the compensation α_n , we first define

$$H(n) = \frac{i^{n-1} (1-\eta)^{\frac{n}{2}}}{2^{\frac{n+1}{2}}}, \quad (\text{A21})$$

and it must satisfy the following relation:

$$\begin{aligned} |H(1)|^2 \alpha_{x-1}^2 &= |H(2)|^2 \alpha_{x-2}^2 = |H(3)|^2 \alpha_{x-3}^2 \\ &= \dots = |H(x)|^2 \alpha_0^2. \end{aligned} \quad (\text{A22})$$

Therefore, we have

$$\alpha_n^2 = \frac{\left(\frac{2}{1-\eta}\right)^{x-n-1}}{\sum_{j=0}^{x-1} \left(\frac{2}{1-\eta}\right)^j}. \quad (\text{A23})$$

In this way, we can successfully compensate for the losses. The extra phases can be corrected by applying phase gates on Bob's qubits. Therefore, we finally achieve m copies of the Bell state $|\Phi^+\rangle = (|0_A 0_B\rangle + |1_A 1_B\rangle)/\sqrt{2}$. Note that this photon erasure approach is probabilistic instead of deterministic, unlike the one introduced in [13]. According to (A20), the

success probability P_{succ} for the switch-free implementation is

$$\begin{aligned} P_{\text{succ}}(m) &= \sum_{k=0}^{\infty} \frac{(1-\eta)^k}{2^k} \left(\sum_{n=1}^{2^m} \frac{(1-\eta)^n}{2^{n+1}} \alpha_{2^m-n}^2 \right) \\ &= \sum_{k=0}^{\infty} \frac{2^{m-k-2} (1-\eta)^{k+1}}{\sum_{j=0}^{2^m-1} \left(\frac{2}{1-\eta}\right)^j}. \end{aligned} \quad (\text{A24})$$

b. Concatenated delay loops

As shown in the main text, the P_{succ} in the single-loop photon erasure is too low. Therefore, one may connect multiple loops and apply the detection at the end, as shown in the bottom of Fig. 2. Suppose there are s photon loops connected, and we denote the operators in each loop as $\widehat{a}^{(0)\dagger}$, $\widehat{a}^{(1)\dagger}$, $\widehat{a}^{(2)\dagger}$, ..., $\widehat{a}^{(s-1)\dagger}$. Note that we have

$$\widehat{a}^{(k)\dagger}_{2,j} = \widehat{a}^{(k+1)\dagger}_{1,j}, \quad (\text{A25})$$

where $k \in \{0, 1, 2, 3, \dots, s-2\}$. By combining the calculations for the single loop and using (A25), we are able to deduce that the input $\widehat{a}^{(0)\dagger}_{1,j}$ satisfies the following Pascal's triangle pattern:

When $s = 1$, the detection happens on $\widehat{a}^{(0)\dagger}_2$,

$$\widehat{a}^{(0)\dagger}_{1,j} = \frac{i}{\sqrt{2}} \widehat{a}^{(0)\dagger}_{2,j} + \sum_{n^{(0)} \geq 1} H(n^{(0)}) \widehat{a}^{(0)\dagger}_{2,j+n^{(0)}} + \text{loss terms}. \quad (\text{A26})$$

When $s = 2$, the detection happens on $\widehat{a}^{(1)\dagger}_2$,

$$\begin{aligned} \widehat{a}^{(0)\dagger}_{1,j} &= \frac{i}{\sqrt{2}} \widehat{a}^{(0)\dagger}_{2,j} + \sum_{n^{(0)} \geq 1} H(n^{(0)}) \widehat{a}^{(0)\dagger}_{2,j+n^{(0)}} + \text{loss terms} \\ &= \frac{i}{\sqrt{2}} \widehat{a}^{(1)\dagger}_{1,j} + \sum_{n^{(0)} \geq 1} H(n^{(0)}) \widehat{a}^{(1)\dagger}_{1,j+n^{(0)}} + \text{loss terms} \\ &= \left(\frac{i}{\sqrt{2}}\right)^2 \widehat{a}^{(1)\dagger}_{2,j} + 2 \frac{i}{\sqrt{2}} \sum_{n^{(0)} \geq 1} H(n^{(0)}) \widehat{a}^{(1)\dagger}_{2,j+n^{(0)}} \\ &\quad + \sum_{n^{(0)}, n^{(1)} \geq 1} H(n^{(0)}) H(n^{(1)}) \widehat{a}^{(1)\dagger}_{2,j+n^{(0)}+n^{(1)}} + \text{loss terms}. \end{aligned} \quad (\text{A27})$$

When $s = 3$, the detection happens on $\widehat{a}^{(2)\dagger}_2$,

$$\begin{aligned} \widehat{a}^{(0)\dagger}_{1,j} &= \left(\frac{i}{\sqrt{2}}\right)^2 \widehat{a}^{(1)\dagger}_{2,j} + 2 \frac{i}{\sqrt{2}} \sum_{n^{(0)} \geq 1} H(n^{(0)}) \widehat{a}^{(1)\dagger}_{2,j+n^{(0)}} + \sum_{n^{(0)}, n^{(1)} \geq 1} H(n^{(0)}) H(n^{(1)}) \widehat{a}^{(1)\dagger}_{2,j+n^{(0)}+n^{(1)}} + \text{loss terms} \\ &= \left(\frac{i}{\sqrt{2}}\right)^2 \widehat{a}^{(2)\dagger}_{1,j} + 2 \frac{i}{\sqrt{2}} \sum_{n^{(0)} \geq 1} H(n^{(0)}) \widehat{a}^{(2)\dagger}_{1,j+n^{(0)}} + \sum_{n^{(0)}, n^{(1)} \geq 1} H(n^{(0)}) H(n^{(1)}) \widehat{a}^{(2)\dagger}_{1,j+n^{(0)}+n^{(1)}} + \text{loss terms} \\ &= \left(\frac{i}{\sqrt{2}}\right)^3 \widehat{a}^{(2)\dagger}_{2,j} + 3 \left(\frac{i}{\sqrt{2}}\right)^2 \sum_{n^{(0)} \geq 1} H(n^{(0)}) \widehat{a}^{(2)\dagger}_{2,j+n^{(0)}} + 3 \frac{i}{\sqrt{2}} \sum_{n^{(0)}, n^{(1)} \geq 1} H(n^{(0)}) H(n^{(1)}) \widehat{a}^{(2)\dagger}_{2,j+n^{(0)}+n^{(1)}} \\ &\quad + \sum_{n^{(0)}, n^{(1)}, n^{(2)} \geq 1} H(n^{(0)}) H(n^{(1)}) H(n^{(2)}) \widehat{a}^{(2)\dagger}_{2,j+n^{(0)}+n^{(1)}+n^{(2)}} + \text{loss terms}. \end{aligned} \quad (\text{A28})$$

One can continue the calculations and get the general formula for any $s \in \mathbb{Z}^+$,

$$\widehat{a}^{(0)\dagger}_{1,j} = \binom{s}{0} \left(\frac{i}{\sqrt{2}}\right)^s \widehat{a}^{(s-1)\dagger}_{2,j} + \sum_{d=1}^s \binom{s}{d} \left(\frac{i}{\sqrt{2}}\right)^{s-d} \left[\sum_{n^{(0)}, \dots, n^{(d-1)} \geq 1} \left(\prod_{\tau=0}^{d-1} H(n^{(\tau)}) \right) \widehat{a}^{(s-1)\dagger}_{2,j+\sum_{k=0}^{d-1} n^{(k)}} \right]. \quad (\text{A29})$$

Now, we perform the actions on the state, i.e., the final state, after the detector clicks. According to the state before photon measurement in (A13), we can calculate the resulting state for each clicking moment. Similar to the single-loop scenario, we obtain the final state,

$$\begin{aligned} |\psi\rangle &= (\text{terms before } |x\rangle_{ph}) + \left(\frac{i}{\sqrt{2}}\right)^{s-1} \sum_{u=x}^{\infty} \left\{ \sum_{n=0}^{x-1} \left[\sum_{k=1}^{\min[s, u-n]} (-1)^{k+1} \binom{s}{k} \binom{u-n-1}{k-1} \right] H(u-n) \alpha_n S_n \right\} |u\rangle_{ph} + (\text{loss terms}) \\ &= (\text{terms before } |x\rangle_{ph}) + \left(\frac{i}{\sqrt{2}}\right)^{s-1} \sum_{u=x}^{\infty} \left\{ \sum_{n=0}^{x-1} [Y(s, u, n) H(u-n) \alpha_n S_n] \right\} |u\rangle_{ph} + (\text{loss terms}) \\ &= (\text{terms before } |x\rangle_{ph}) + \sum_{u=x}^{\infty} \left\{ \left(\frac{i^{s+u-2} \sqrt{1-\eta}^u}{\sqrt{2}^{s+u}} \right) \sum_{n=0}^{x-1} \left(\frac{\sqrt{2}}{i\sqrt{1-\eta}} \right)^n Y(s, u, n) \alpha_n S_n \right\} |u\rangle_{ph} + (\text{loss terms}), \end{aligned} \quad (\text{A30})$$

where we define

$$Y(s, u, k) = \sum_{t=1}^{\min[s, u-k]} (-1)^{t+1} \binom{s}{t} \binom{u-k-1}{t-1}. \quad (\text{A31})$$

Note that the index k is upper bounded by $\min[s, u-n]$ since, practically, we do not have an infinitely large number of loops s . Thus, some of the terms in (A29) may be truncated. Still, we have the terms in a nicely formed summation until the clicking time bin is at or after $|x\rangle_{ph}$. However, it does not guarantee that we have good states. In order to make the state without information loss and phase correctable (i.e., the terms before each S_n are nonzero and have the same sign), we must choose a suitable integer set (s, u) such that $Y(s, u, n)$ has the same sign throughout all n , i.e.,

$$Y(s, u, n) > 0 \text{ or } Y(s, u, n) < 0 \\ \text{for } \forall n \in \{0, 1, 2, \dots, x-1\}. \quad (\text{A32})$$

In this way, we can compensate for the amplitude of the photonic pulses, which should satisfy

$$\begin{aligned} \left| Y(s, u, 0) \frac{(1-\eta)^{-\frac{0}{2}}}{2^{-\frac{0}{2}}} \alpha_0 \right|^2 &= \left| Y(s, u, 1) \frac{(1-\eta)^{-\frac{1}{2}}}{2^{-\frac{1}{2}}} \alpha_1 \right|^2 \\ &= \left| Y(s, u, 2) \frac{(1-\eta)^{-\frac{2}{2}}}{2^{-\frac{2}{2}}} \alpha_2 \right|^2 \\ &= \dots = \\ &= \left| Y(s, u, x-1) \frac{(1-\eta)^{-\frac{x-1}{2}}}{2^{-\frac{x-1}{2}}} \alpha_{x-1} \right|^2. \end{aligned} \quad (\text{A33})$$

Therefore, according to the equation above and the normalization condition $\sum_{n=0}^{2^m-1} \alpha_n^2 = 1$, we can obtain the amplitude compensation term,

$$\alpha_n^2 = \frac{1}{\sum_{k=0}^{x-1} \left| \frac{Y(s, u, n)}{Y(s, u, k)} \right|^2 \left(\frac{1-\eta}{2} \right)^{k-n}}. \quad (\text{A34})$$

In this way, when the detector clicks at time bin u , we can acquire the state (9) and transform it to m copies of the Bell state by applying phase correction single-qubit gates. According to (A30), when we fix the number of connected loops s and the clicking time bin u , the corresponding photon erasure success probability (regardless of qubit-qudit entanglement local losses and transmission loss) is

$$P_{\text{succ}}(s, u, m) = \frac{x(1-\eta)^u}{2^{s+u}} \frac{1}{\sum_{k=0}^{x-1} \left| \frac{1}{Y(s, u, k)} \right|^2 \left(\frac{1-\eta}{2} \right)^k}. \quad (\text{A35})$$

Note that in this case, since α_n depends on u and s and we need to generate the pulses according to α_n at the very beginning of the protocol, we need to choose only one clicking time bin as the success flag. Therefore, one needs to find the best (s, u) set that outputs the maximum $P_{\text{succ}}(s, u, m)$.

Additionally, the above calculations for the concatenated loops also fit the case for the single loop where $s = 1$. The only change to make is that one needs to sum over all the success probabilities P_{succ} for the clicking time $u \geq x$ as

the erasure success probability for the single loop, i.e.,

$$P_{\text{succ}}(s = 1, m) = \sum_{u=x}^{\infty} P_{\text{succ}}(s = 1, u, m). \quad (\text{A36})$$

c. Photon measurement with loss

Generally, the loss of the photon can happen during the local qubit-qudit interaction, the transmission between Alice and Bob, and the delay loop of the photon erasure.

The fidelity of the resulting state will not be affected by the previous two losses since the photon is subject to the same amount of losses regardless of which time bin it is in. Therefore, they do not contribute any correlated errors, but will only lower the success probability of the protocol. The local losses increase with the number of entangled pairs such that the total loss probability from the qudit-qubit interactions is $(1 - \eta_{AB})^m$, where η_{AB} is the loss per interaction. The transmission probability between Alice and Bob is denoted as $1 - \eta_0$ and we assume fiber loss at telecom frequencies.

For the third kind of photon losses—the losses in the delay loops of the photon erasure—they lower the success probability but they also affect the fidelity of the generated pairs since each qudit pulse may also experience a different number of delay loops. Nevertheless, we can choose the compensation coefficients α_n in Eq. (A34), which will vary with the loss on each delay loop η as well. As a result, the success probability for photon measurement will change correspondingly. The overall success probability P_{total} is

$$P_{\text{total}} = (1 - \eta_{AB})^m (1 - \eta_0) P_{\text{succ}}, \quad (\text{A37})$$

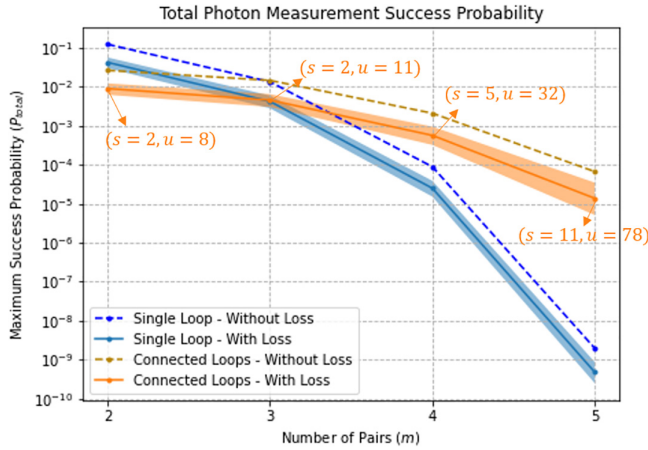
where P_{succ} is defined in (A36) for $s = 1$ and (A35) for $s \geq 2$. Now, we can input some moderate loss parameters for η , η_{AB} , and η_0 to discuss the P_{total} .

First, we assume the photon wavelength is in the range of $\sim 600\text{--}800$ nm, corresponding to typical optical transitions of relevant quantum hardware such as group-IV diamond defect centers. For the transmission between Alice and Bob, the photon will have to be frequency converted to the telecom band for efficient transmission in low-loss optical fibers before being converted back to $\sim 600\text{--}800$ nm for interaction with Bob's qubits. We assume that after interaction with Bob's qubits, the wavelength is kept at $\sim 600\text{--}800$ nm for the erasure measurement. Assuming fiber delay lines, the loss is $\sim 5\text{--}10$ dB/km [36] for this wavelength range.

Assuming that the time-bin duration is approximately 70 ns [22,24] and the transmission velocity of the photon in the fiber is 2×10^5 km/s, we find that the dB loss on each delay loop is $\sim 0.07\text{--}0.14$ dB and the corresponding loss percentage is $\eta \sim 0.0160\text{--}0.0317$.

Assuming frequency conversion to the telecom band for the transmission between Alice and Bob, the transmission loss will be $\sim 0.15\text{--}0.25$ dB/km [37] and result in a transmission of $\eta_0 \sim 0.499\text{--}0.684$ for 20 km separation. We also assume $\eta_{AB} \sim 0.05\text{--}0.10$ for a general approximation of the local losses.

With these parameters and according to P_{total} , one can find the total photon measurement success probability, as shown in Fig. 9. We can find that P_{total} will, of course, drop when the number of generated pairs increases. Moreover, for the



Total probability: $P_{total} = (1 - \eta_{AB})^m (1 - \eta_0) P_{succ}$
 $\eta_{AB} = 5\% \sim 10\%$
 $\eta_0 = 49.9\% \sim 68.4\% \rightarrow 3dB \sim 5dB$
 $\eta = 1.60\% \sim 3.17\% \rightarrow 0.07dB \sim 0.14dB$
 s (# loops) range for connected loops: $2 \sim 15$
 u (# clicking time) range for connected loops: $2^m \sim 2^m + 50$

FIG. 9. The total success probability of the photon erasure with respect to the number of generated pairs ($m \sim 2-5$) is shown. We consider both the single-loop and the connected-loops cases. We define the possible parameter ranges for the losses, s and u , and then find the maximum P_{total} . The applied (s, u) 's are marked on the plot. Connecting photon loops increases the total measurement success probability compared to the case where only one single-photon loop is placed. Note that for a single-photon loop, the success probability refers to (A36). The cases where no loss occurs are also plotted for the comparisons.

single-photon loop, the P_{total} drops drastically, which will make the measurement vulnerable to the detector's dark count rate ($\sim 10^{-7} - 10^{-6}$). However, with photon loops connected, the drop of the P_{total} can be slightly mitigated, making the measurement more resistant to the dark count.

4. Quantum memory

Qubits are vulnerable to decoherence. To simulate qubit decoherence during transmission, we employ a dephasing and generalized amplitude damping channel. Suppose the distance between Alice and Bob is L ; the speed of photon transmission between them is represented by c . In this scenario, Alice must send the photon to Bob and wait for the heralding information to return. Additionally, we define the success of the protocol based on Alice receiving Bob's heralding message. Therefore, the waiting time t for Alice is

$$t_A = \frac{2L}{c}, \quad (A38)$$

and for Bob, it is

$$t_B = \frac{L}{c}. \quad (A39)$$

Suppose the dephasing time is T_p ; then the Kraus operators of the dephasing channel are

$$A_0 = \sqrt{\frac{1 + e^{-t/T_p}}{2}} \mathbf{I}, \quad A_1 = \sqrt{\frac{1 - e^{-t/T_p}}{2}} \mathbf{Z}, \quad (A40)$$

where \mathbf{I} and \mathbf{Z} denote the identity and Pauli-Z matrix, respectively. Also, by indicating the relaxation time T_1 , the Kraus operators of the amplitude damping channel are

$$\begin{aligned}
 E_0 &= \sqrt{a_\beta} \begin{bmatrix} 1 & 0 \\ 0 & e^{-t/2T_1} \end{bmatrix}, \\
 E_1 &= \sqrt{a_\beta} \begin{bmatrix} 0 & \sqrt{1 - e^{-t/T_1}} \\ 0 & 0 \end{bmatrix}, \\
 E_2 &= \sqrt{1 - a_\beta} \begin{bmatrix} e^{-t/2T_1} & 0 \\ 0 & 1 \end{bmatrix}, \\
 E_3 &= \sqrt{1 - a_\beta} \begin{bmatrix} 0 & 0 \\ \sqrt{1 - e^{-t/T_1}} & 0 \end{bmatrix}, \quad (A41)
 \end{aligned}$$

where

$$a_\beta = e^{-\beta \Delta E} = e^{-\frac{\Delta E}{k_B T}}, \quad (A42)$$

and ΔE , k_B , and T denote the energy difference between $|0\rangle$ and $|1\rangle$, Boltzmann constant, and system temperature, respectively. Therefore, by applying the two kinds of Kraus operators, the output density matrix ρ becomes

$$\rho' = \sum_{i=0,1; j=0,1,2,3} A_i E_j \rho E_j^\dagger A_i^\dagger. \quad (A43)$$

We set $L = 20$ km, $T_1 = 10$ ms, $T_p = 5$ ms, and $a_\beta = 0.5$. Note that this is the case for only one qubit. For a multiqubit system, since the decoherence channels on each qubit are uncorrelated, we can apply Eq. (A43) on each qubit independently.

Notably, despite the errors mentioned above, qubit gate errors should also be considered, especially for the latter one since we put a lot of HADAMARD operations inside.

APPENDIX B: GENETIC PURIFICATION PROTOCOL

In this Appendix, we show the basic idea of the optimized purification protocol proposed in [17].

1. Error detection by measurement

Consider that the noises on the entangled pairs are described as depolarizing errors,

$$\begin{aligned}
 \rho_{AB} &= (1 - x_0 - y_0 - z_0) |\Phi^+\rangle \langle \Phi^+| + x_0 |\Psi^+\rangle \langle \Psi^+| \\
 &\quad + y_0 |\Psi^-\rangle \langle \Psi^-| + z_0 |\Phi^-\rangle \langle \Phi^-|. \quad (B1)
 \end{aligned}$$

Similar to the conventional depolarizing channel, we input I (no errors), X , Y , or Z errors into the perfect state with the corresponding possibilities. For the Bell pair case, the desired perfect state is $|\Phi^+\rangle$ and the other three erroneous states are

$$\begin{aligned}
 |\Psi^+\rangle &= \frac{1}{\sqrt{2}} (|01\rangle + |10\rangle) \rightarrow \mathbf{X} \text{ error}, \\
 |\Psi^-\rangle &= \frac{1}{\sqrt{2}} (|01\rangle - |10\rangle) \rightarrow \mathbf{Y} \text{ error}, \\
 |\Phi^-\rangle &= \frac{1}{\sqrt{2}} (|00\rangle - |11\rangle) \rightarrow \mathbf{Z} \text{ error}. \quad (B2)
 \end{aligned}$$

Note that in the output states, there may also exist some coherent errors (e.g., $|\Phi^+\rangle \langle \Psi^-|$). These errors can be eliminated by using the twirling error mitigation technique [38].

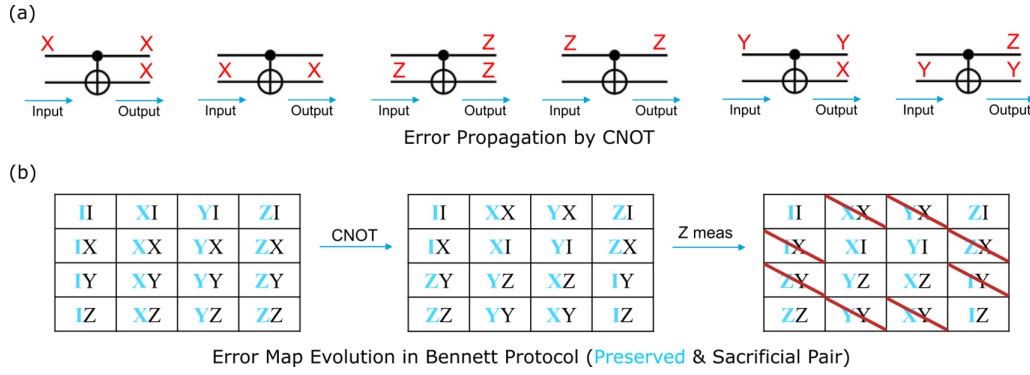


FIG. 10. (a) How CNOT propagates the input errors. (b) The error map evolution within the Bennett protocol [9].

However, for the discussions in our work, we will not add the twirling process but implement the purification only.

If Alice and Bob then measure their own register qubits separately, they will know whether or not their previous shared entangled pair has errors. There are three possible measurement blocks that Alice and Bob can choose:

- (i) Measurement in X basis,
- (ii) Measurement in Y basis,
- (iii) Measurement in Z basis,

and there are two possible measurement results from Alice and Bob:

- (i) Coincidence result: $0_A 0_B$ and $1_A 1_B$,
- (ii) Anticoincidence result: $0_A 1_B$ and $1_A 0_B$.

Note that the measurement on one certain basis can only detect two kinds of errors. For example, by applying the X -basis measurement, only Y and Z can be detected. Also, one should always preserve $|\Phi^+\rangle$ and cannot consider it as one of the erroneous states. Therefore, if Alice and Bob want to know whether their previous shared ρ_{AB} is possibly in $|\Phi^+\rangle$, their measurement results and measurement basis should obey the criteria as follows:

- (a) Measurement in X basis: Coincidence result $\rightarrow |\Psi^-\rangle$ and $|\Phi^-\rangle$ detectable.
- (b) Measurement in Y basis: Anticoincidence result $\rightarrow |\Psi^+\rangle$ and $|\Phi^-\rangle$ detectable.
- (c) Measurement in Z basis: Coincidence result $\rightarrow |\Psi^-\rangle$ and $|\Psi^+\rangle$ detectable.

If the measurement result of Alice and Bob violates the above criteria, then Alice and Bob will know that their previous shared pair ρ_{AB} is in one of the erroneous states.

2. Error propagation

By directly measuring the entangled pair, we are indeed able to detect the errors inside the Bell pair, but, in the meantime, also destroy the entanglement. In order to make errors detectable without entanglement demolition, one should introduce another sacrificial entangled pair. Alice and Bob can then apply CNOTs locally to connect the preserved and sacrificial pair and propagate the errors in the preserved pair to the sacrificial pair, as shown in Fig. 10(a). The final measurement check will be applied to the sacrificial pairs to detect and eliminate errors.

Consider the simplest purification protocol: the Bennett protocol [9]. Suppose both pairs are modeled as the

depolarizing channel, as shown in Eq. (B1), and the error map is shown in Fig. 10(b). The CNOT will change the error map according to the error propagation in Fig. 10(a). The final Z -basis measurement will eliminate the blocks with X and Y errors on the sacrificial pair.

3. Error permutation

The error propagation indeed provides the approach to send the larger errors to the sacrificial pair and eliminate them by measurements. However, the freedom of controlling the error flow is still limited.

The error permutation is a technique that permutes the error coefficients by letting Alice and Bob apply the corresponding operations locally. The coefficient permutation and the corresponding single-qubit gate operations on Alice and Bob are shown in Fig. 11. For example, if Alice and Bob apply nothing, the density matrix will remain the same as Eq. (B1). However, if Alice and Bob apply a HADAMARD gate, respectively, the shared density matrix will become

$$\rho_{AB} = (1 - x_0 - y_0 - z_0)|\Phi^+\rangle\langle\Phi^+| + z_0|\Psi^+\rangle\langle\Psi^+| + y_0|\Psi^-\rangle\langle\Psi^-| + x_0|\Phi^-\rangle\langle\Phi^-|, \quad (\text{B3})$$

which applies the exchange between x_0 and z_0 . Suppose z_0 is much larger than x_0 and y_0 and we still keep the Z -basis measurement. In Eq. (B1), we can only eliminate $|\Psi^+\rangle$ and $|\Psi^-\rangle$ affiliated with x_0 and y_0 . However, if we apply the permutation shown above, $|\Psi^+\rangle$ and $|\Psi^-\rangle$ will still be eliminated, but they are affiliated with z_0 and y_0 . In this way, we flow the erroneous states with the largest coefficient into the error detection part without changing the measurement basis.

4. Evolutionary algorithm

We already have different measurement blocks, error propagation, and permutation techniques. Now, we should assemble these components to find the optimal purification circuit. Note that the circuit is designed only for one-round purification. It means that we implement the aforementioned components into the whole local m -qubit system. Then, the evolutionary algorithm is adopted to search for an optimized purification protocol. The procedure is shown as follows:

- (i) Completely randomize the initial circuit group by stochastically assembling the CNOTs, permutation gates, and measurement blocks.

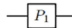
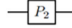
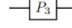
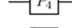
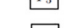
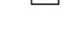
States	Alice	Bob	
$\rho_1 = (1 - x_0 - y_0 - z_0) \phi_+\rangle\langle\phi_+ + x_0 \psi_+\rangle\langle\psi_+ + y_0 \psi_-\rangle\langle\psi_- + z_0 \phi_-\rangle\langle\phi_- $	None	None	
$\rho_2 = (1 - x_0 - y_0 - z_0) \phi_+\rangle\langle\phi_+ + x_0 \psi_+\rangle\langle\psi_+ + y_0 \psi_-\rangle\langle\psi_- + z_0 \phi_-\rangle\langle\phi_- $	H	H	
$\rho_3 = (1 - x_0 - y_0 - z_0) \phi_+\rangle\langle\phi_+ + x_0 \psi_+\rangle\langle\psi_+ + z_0 \psi_-\rangle\langle\psi_- + y_0 \phi_-\rangle\langle\phi_- $	HS	SH	
$\rho_4 = (1 - x_0 - y_0 - z_0) \phi_+\rangle\langle\phi_+ + z_0 \psi_+\rangle\langle\psi_+ + x_0 \psi_-\rangle\langle\psi_- + y_0 \phi_-\rangle\langle\phi_- $	SH	(HS) ²	
$\rho_5 = (1 - x_0 - y_0 - z_0) \phi_+\rangle\langle\phi_+ + y_0 \psi_+\rangle\langle\psi_+ + z_0 \psi_-\rangle\langle\psi_- + x_0 \phi_-\rangle\langle\phi_- $	(SH) ²	(HS) ⁴	
$\rho_6 = (1 - x_0 - y_0 - z_0) \phi_+\rangle\langle\phi_+ + y_0 \psi_+\rangle\langle\psi_+ + x_0 \psi_-\rangle\langle\psi_- + z_0 \phi_-\rangle\langle\phi_- $	H(SH) ²	S(HS) ³	

FIG. 11. The error permutation and the corresponding single-qubit gate operations applied on Alice and Bob.

(ii) Input the Bell pair state with the specific error model in the purification circuits, and output the fidelity of the purified Bell pair for all purification circuits. Select the best purification circuits (more than one).

(iii) Consider that the selected circuits are the parent circuits, and the operations on the circuits are their genes. Let the parent circuits reproduce baby circuits by randomly mixing the genes from their parents.

(iv) The selected circuits and the baby circuits form the new circuit group.

(v) Since no new genes (operations) are involved, the mutations should be introduced, i.e., some of the operations are mutated to another random different operation with relatively low probabilities among all circuits in the newly formed group.

(vi) Output the purified fidelity in the circuits from the mutated group.

(vii) Loop it back to the parent circuit selection step and continue the loop hundreds of times until the maximum purified fidelity reaches convergence.

(viii) The purification circuit with the converged fidelity will be the optimized purification circuit for the specific error model.

Note that all of the purified circuits and the following output results are under the condition of the minimum entanglement requirement. The minimum entanglement requirement means using the minimum number of CNOTs to connect all shared Bell pairs without leaving any pair unoperated. One can indeed set the purified circuits to a larger size and run the algorithm, but with more local two-qubit gate consumptions.

[1] S. Pirandola, U. L. Andersen, L. Banchi, M. Berta, D. Bunandar, R. Colbeck, D. Englund, T. Gehring, C. Lupo, C. Ottaviani *et al.*, Advances in quantum cryptography, *Adv. Opt. Photon.* **12**, 1012 (2020).

[2] C. L. Degen, F. Reinhard, and P. Cappellaro, Quantum sensing, *Rev. Mod. Phys.* **89**, 035002 (2017).

[3] Z. Zhang and Q. Zhuang, Distributed quantum sensing, *Quantum Sci. Technol.* **6**, 043001 (2021).

[4] X. Guo, C. R. Breum, J. Borregaard, S. Izumi, M. V. Larsen, T. Gehring, M. Christandl, J. S. Neergaard-Nielsen, and U. L. Andersen, Distributed quantum sensing in a continuous-variable entangled network, *Nat. Phys.* **16**, 281 (2020).

[5] R. Beals, S. Brierley, O. Gray, A. W. Harrow, S. Kutin, N. Linden, D. Shepherd, and M. Stather, Efficient distributed quantum computing, *Proc. R. Soc. A* **469**, 20120686 (2013).

[6] A. S. Cacciapuoti, M. Caleffi, F. Tafuri, F. S. Cataliotti, S. Gherardini, and G. Bianchi, Quantum internet: Networking challenges in distributed quantum computing, *IEEE Network* **34**, 137 (2019).

[7] H. Buhrman and H. Röhrig, Distributed quantum computing, in *International Symposium on Mathematical Foundations of Computer Science*, MFCS 2003, Lecture Notes in Computer Science, Vol. 2747 (Springer, Berlin, Heidelberg, 2003), pp. 1–20.

[8] D. Awschalom, K. K. Berggren, H. Bernien, S. Bhave, L. D. Carr, P. Davids, S. E. Economou, D. Englund, A. Faraon, M. Fejer, S. Guha, M. V. Gustafsson, E. Hu, L. Jiang, J. Kim, B. Kozh, P. Kumar, P. G. Kwiat, M. Lončar, M. D. Lukin *et al.*, Development of quantum interconnects (Quics) for next-generation information technologies, *PRX Quantum* **2**, 017002 (2021).

[9] C. H. Bennett, G. Brassard, S. Popescu, B. Schumacher, J. A. Smolin, and W. K. Wootters, Purification of noisy entanglement and faithful teleportation via noisy channels, *Phys. Rev. Lett.* **76**, 722 (1996).

[10] D. Deutsch, A. Ekert, R. Jozsa, C. Macchiavello, S. Popescu, and A. Sanpera, Quantum privacy amplification and the security of quantum cryptography over noisy channels, *Phys. Rev. Lett.* **77**, 2818 (1996).

[11] A. G. Fowler, D. S. Wang, C. D. Hill, T. D. Ladd, R. Van Meter, and L. C. L. Hollenberg, Surface code quantum communication, *Phys. Rev. Lett.* **104**, 180503 (2010).

[12] A. Javadi-Abhari, P. Gokhale, A. Holmes, D. Franklin, K. R. Brown, M. Martonosi, and F. T. Chong, Optimized surface code communication in superconducting quantum computers, in *Proceedings of the 50th Annual IEEE/ACM International Symposium on Microarchitecture* (IEEE, Piscataway, NJ, 2017), pp. 692–705.

[13] Y. Zheng, H. Sharma, and J. Borregaard, Entanglement distribution with minimal memory requirements using time-bin photonic qudits, *PRX Quantum* **3**, 040319 (2022).

[14] Z. Xie, Y. Liu, X. Mo, T. Li, and Z. Li, Quantum entanglement creation for distant quantum memories via time-bin multiplexing, *Phys. Rev. A* **104**, 062409 (2021).

[15] N. Lo Piparo, W. J. Munro, and K. Nemoto, Quantum multiplexing, *Phys. Rev. A* **99**, 022337 (2019).

[16] H. Zhou, T. Li, K. Xia *et al.*, Parallel and heralded multiqubit entanglement generation for quantum networks, *Phys. Rev. A* **107**, 022428 (2023).

- [17] S. Krastanov, V. V. Albert, and L. Jiang, Optimized entanglement purification, *Quantum* **3**, 123 (2019).
- [18] E. Knill, R. Laflamme, and G. J. Milburn, A scheme for efficient quantum computation with linear optics, *Nature (London)* **409**, 46 (2001).
- [19] E. Knill, Quantum computing with realistically noisy devices, *Nature (London)* **434**, 39 (2005).
- [20] R. Namiki, L. Jiang, J. Kim, and N. Lütkenhaus, Role of syndrome information on a one-way quantum repeater using teleportation-based error correction, *Phys. Rev. A* **94**, 052304 (2016).
- [21] S. J. Devitt, W. J. Munro, and K. Nemoto, Quantum error correction for beginners, *Rep. Prog. Phys.* **76**, 076001 (2013).
- [22] E. N. Knall, C. M. Knaut, R. Bekenstein, D. R. Assumpcao, P. L. Stroganov, W. Gong, Y. Q. Huan, P.-J. Stas, B. Machielse, M. Chalupnik, D. Levonian, A. Suleymanzade, R. Riedinger, H. Park, M. Lončar, M. K. Bhaskar, and M. D. Lukin, Efficient source of shaped single photons based on an integrated diamond nanophotonic system, *Phys. Rev. Lett.* **129**, 053603 (2022).
- [23] L.-M. Duan and H. J. Kimble, Scalable photonic quantum computation through cavity-assisted interactions, *Phys. Rev. Lett.* **92**, 127902 (2004).
- [24] M. K. Bhaskar, R. Riedinger, B. Machielse, D. S. Levonian, C. T. Nguyen, E. N. Knall, H. Park, D. Englund, M. Lončar, D. D. Sukachev *et al.*, Experimental demonstration of memory-enhanced quantum communication, *Nature (London)* **580**, 60 (2020).
- [25] W. Dür and H. J. Briegel, Entanglement purification and quantum error correction, *Rep. Prog. Phys.* **70**, 1381 (2007).
- [26] S. Muralidharan, L. Li, J. Kim, N. Lütkenhaus, M. D. Lukin, and L. Jiang, Optimal architectures for long distance quantum communication, *Sci. Rep.* **6**, 20463 (2016).
- [27] C. Monroe, R. Raussendorf, A. Ruthven, K. R. Brown, P. Maunz, L.-M. Duan, and J. Kim, Large-scale modular quantum-computer architecture with atomic memory and photonic interconnects, *Phys. Rev. A* **89**, 022317 (2014).
- [28] Z.-J. Zhang and Z.-X. Man, Many-agent controlled teleportation of multi-qubit quantum information, *Phys. Lett. A* **341**, 55 (2005).
- [29] Y.-h. Li, X.-l. Li, L.-p. Nie, and M.-h. Sang, Quantum teleportation of three and four-qubit state using multiqubit cluster states, *Intl. J. Theor. Phys.* **55**, 1820 (2016).
- [30] R. Laflamme, C. Miquel, J. P. Paz, and W. H. Zurek, Perfect quantum error correcting code, *Phys. Rev. Lett.* **77**, 198 (1996).
- [31] M. Grassl, T. Beth, and T. Pellizzari, Codes for the quantum erasure channel, *Phys. Rev. A* **56**, 33 (1997).
- [32] J. P. Lee, L. M. Wells, B. Villa, S. Kalliakos, R. M. Stevenson, D. J. P. Ellis, I. Farrer, D. A. Ritchie, A. J. Bennett, and A. J. Shields, Controllable photonic time-bin qubits from a quantum dot, *Phys. Rev. X* **8**, 021078 (2018).
- [33] H. Sharma, Scattering based scheme for generation of photonic tree-cluster states, Master's thesis, TUDelft, 2022, <https://repository.tudelft.nl/islandora/object/uuid:64e71ea0-2f72-4f35-b253-8a80326fd7af?collection=education>.
- [34] K. Tiurev, P. L. Mirambell, M. B. Lauritzen, M. H. Appel, A. Tiranov, P. Lodahl, and A. S. Sørensen, Fidelity of time-bin-entangled multiphoton states from a quantum emitter, *Phys. Rev. A* **104**, 052604 (2021).
- [35] C.-P. Yang, Shih-I. Chu, and S. Han, Simplified realization of two-qubit quantum phase gate with four-level systems in cavity QED, *Phys. Rev. A* **70**, 044303 (2004).
- [36] Thorlabs fiber parameters, <https://www.thorlabs.com>.
- [37] M.-J. Li and T. Hayashi, Advances in low-loss, large-area, and multicore fibers, in *Optical Fiber Telecommunications VII* (Elsevier, Amsterdam, 2020), pp. 3–50.
- [38] M. R. Geller and Z. Zhou, Efficient error models for fault-tolerant architectures and the Pauli twirling approximation, *Phys. Rev. A* **88**, 012314 (2013).